



Technical Note

# A Decade from the Costa Concordia Shipwreck: Lesson Learned on the Contribution of Infrared Thermography during the Maritime Salvage Operations

William Frodella <sup>1,\*</sup>, Guglielmo Rossi <sup>2</sup>, Luca Tanteri <sup>2</sup>, Ascanio Rosi <sup>3</sup>, Luca Lombardi <sup>1</sup>,  
Francesco Mugnai <sup>4</sup>, Riccardo Fanti <sup>1</sup> and Nicola Casagli <sup>1</sup>

<sup>1</sup> Department of Earth Sciences, University of Florence, Via G. La Pira 4, 50121 Florence, Italy

<sup>2</sup> Civil Protection Centre, University of Florence, Largo Fermi 1, 50142 Florence, Italy

<sup>3</sup> Department of Geosciences, University of Padua, Via G. Gradenigo 6, 35131 Padua, Italy

<sup>4</sup> Department of Civil and Environmental Engineering, University of Florence, Via di Santa Marta 3, 50139 Florence, Italy

\* Correspondence: william.frodella@unifi.it; Tel.: +39-055-2755979

**Abstract:** On 13 January 2012, the Italian vessel Costa Concordia wrecked on the shore of Giglio Island, about 15 km off the coast of southern Tuscany (Italy), causing the loss of 32 lives. It is considered one of the worst disasters in maritime history. Salvage operations started immediately after the wreck with the coordination of the Italian National Civil Protection Department and the technological support of several Research Centers, which were activated for the management of the consequent emergency phase. A multi-parametric and multiplatform monitoring system was promptly implemented, involving several advanced remote sensing techniques, among which was Infrared Thermography (IRT). In this framework, IRT monitoring was performed during a 35-day period (25 January–1 March 2012), using a terrestrial, hand-held thermal camera. Six different thermal images were acquired daily from the island's coastline in three different positions, both in daylight and night times. The aim was to detect thermal anomalies connected to possible deformations of the vessel and oil spills. Between 3–4 February, IRT successfully revealed an oil spill drifting from the stern of the wreck towards the island harbor. Furthermore, the wreck's thermal dilatation was also analyzed during a 24-day close-range monitoring, providing interesting insights for the interpretation of the deformation monitoring results. This paper presents the outcomes of these innovative and experimental monitoring activities, with the aim of testing the potential of IRT as a versatile and operative tool to be used in maritime and environmental disaster response.

**Keywords:** shipwreck monitoring; infrared thermography; Costa Concordia; oil spill detection; maritime disaster response



**Citation:** Frodella, W.; Rossi, G.; Tanteri, L.; Rosi, A.; Lombardi, L.; Mugnai, F.; Fanti, R.; Casagli, N. A Decade from the Costa Concordia Shipwreck: Lesson Learned on the Contribution of Infrared Thermography during the Maritime Salvage Operations. *Remote Sens.* **2023**, *15*, 1347. <https://doi.org/10.3390/rs15051347>

Academic Editors: Zhixiang Fang, Quanyi Huang, Jaroslaw Tęgowski, Magaly Koch and Yukiharu Hisaki

Received: 20 January 2023

Revised: 21 February 2023

Accepted: 24 February 2023

Published: 28 February 2023



**Copyright:** © 2023 by the authors. Licensee MDPI, Basel, Switzerland. This article is an open access article distributed under the terms and conditions of the Creative Commons Attribution (CC BY) license (<https://creativecommons.org/licenses/by/4.0/>).

## 1. Introduction

Shipwrecks can often have major economic and ecological impacts in marine and oceanic waters, as well as in anthropic and natural coastal environments. Oil spills connected to shipwrecks, unfortunately, represent a frequent occurrence and are considered as one of the most vital public issues [1–3]. Regarding oil spills in the sea, remote sensing is playing an increasingly important role as a fundamental tool, since it can provide information on the oil-spill movement through multi-temporal imaging [4,5].

This can then be input to drift-prediction models or used to plan effective countermeasures by the response team [6]. Satellite imagery may provide useful overviews on known and very large spills, using either SAR [7–10] or hyperspectral and multispectral data [11–14]. In this context, due to the coarser spatial resolution, thermal data are less adopted [15–18], while optical sensors offer only marginal capability for oil spill detection [19,20]. In the field of small oil spill detection, mapping and monitoring are common

methods often carried out with video or photography from airborne platforms, including Unmanned Aerial Vehicles (UAVs) [5]. In this framework, multispectral [21,22] and thermographic applications [23–25] are present, but still limited, while terrestrial applications, due to logistic and acquisition problems, cannot provide a full coverage of the Areas of Interest (AoIs) [18]. Extensive overviews on the topic of oil spill monitoring are given by [6,9,26–30].

On 13 January 2012, during a cruise in the Mediterranean Sea, the Italian vessel Costa Concordia wrecked offshore of Giglio Island, along the coast of southern Tuscany (Central Italy) (Figure 1a–c). After deviating from the planned route, the ship struck an underwater rock located a few hundred meters east of the island coastline, in front of Giglio Porto locality (Figure 1b). The impact opened a large gash in the ship's portside below the water line, which caused the cutting of the engines' power and the consequent ship drifting towards the island coastline. Luckily, the ship grounded near shore, in a precarious position on a rocky underwater ledge, in front of Gabbianara Point (Figure 1d), where it stood until its removal in July 2014. It is the passenger ship of the largest tonnage to have suffered this consequence; of more than 3229 passengers and 1023 crew, 32 unfortunately died [31].

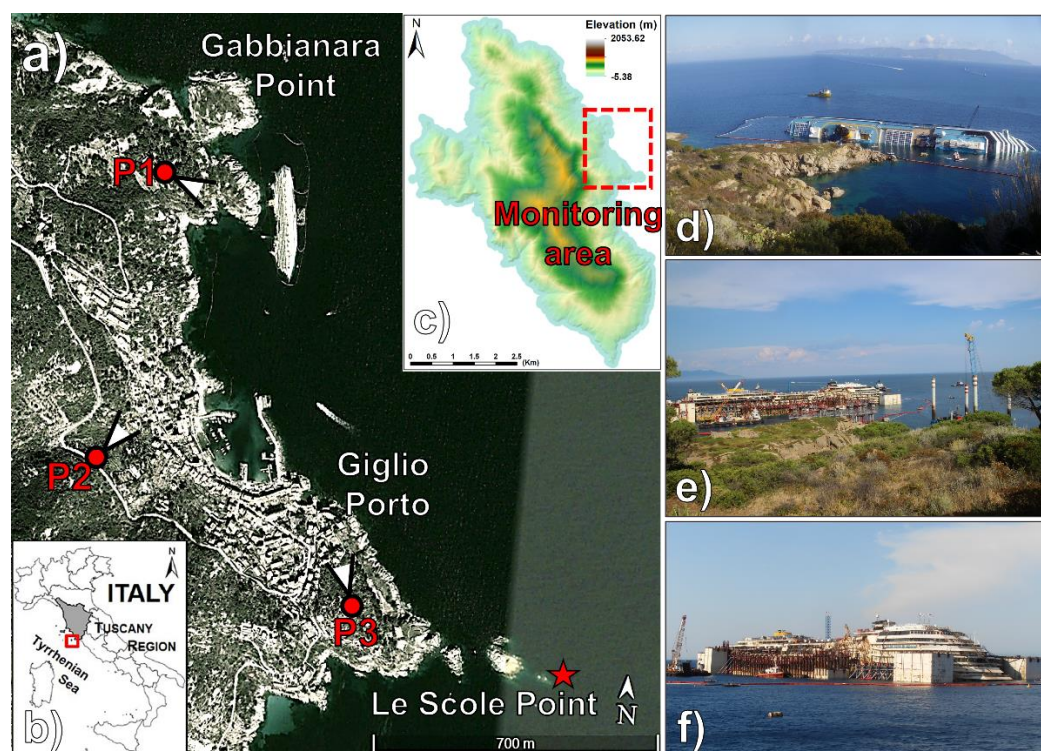


**Figure 1.** Setting of the study area: (a) location of the Costa Concordia after the wreck on Google Earth™ satellite image (March 2012) showing the IRT survey points (P1 = Lazzaretto Point; P2 = Giglio Castello road; P3 = Cannelle); (b) geographic setting of the Giglio island (Tuscany/Central Italy); (c) elevation map of Giglio Island (red dashed square shows the monitoring area). Pictures of the Costa Concordia shipwreck: (d) soon after the wreck in January 2012; (e) during the parbuckling operations in September 2013; (f) in the hull-removal phase (July 2013).

#### *The Costa Concordia Maritime Disaster Management*

Soon after the wreck, salvage operations were set up by the Italian National Civil Protection Department in close coordination with the technical mission structure of the Commissioner delegate, with the technical support of Tuscany Region Central Functional Center, several research centers, and specialized companies. The management of the emergency salvage phases (the largest of this kind to date in maritime disaster history) developed as follows:

- defueling and caretaking (carried out from 18 January 2012 to 15 September 2013): this phase had the primary objective of removing the fuel from the vessel's tanks and engine rooms as quickly as possible, in order to ensure the protection of the marine environment by cleaning of the seabed from the shipwreck debris (Figure 1d);
- parbuckling and post—parbuckling (from 16 September to 31 December 2013): this phase developed with the initial righting of the wreck by rotating the vessel around the longitudinal axis of the ship using cables, giant inflatable buoys, and ballasting with sponsons (Figure 1e);
- hull removal—scrapping (from 31 December 2013 to 14 July 2014): after the hull removal, the Costa Concordia was dragged away from the Giglio Island, to sail for its final cruise to the port of Genoa, where it was finally scrapped [4] (Figure 1f).

During these phases, search and rescue operations were also carried out to extract the victims from the wreck. Especially during the first defueling and caretaking phases, there was a serious concern regarding possible ship displacement and deformations, which in turn could have caused both the sliding of the wreck from the underwater ledge towards the deeper seabed or oil spills. Both hypotheses represented catastrophic scenarios, not only for the rescue teams, but also for the environmental consequences (Giglio Island is in fact part of the protected area of the Tuscan Archipelago National Park). In this framework, in order to ensure the highest safety conditions for the workers and the rescuers operating around and within the wreck, as well as to support the shipwreck removal operations, a multiparametric and multiplatform monitoring system based on-site devices, satellite, and terrestrial remote monitoring techniques was implemented. Amongst traditional seismic [32], topographic [33], and GPS monitoring, several advanced remote sensing techniques were employed, such as space-borne Synthetic Aperture Radar (SAR) satellite [5,34] and ground-based interferometry [35], terrestrial laser scanning, and terrestrial Infrared Thermography (IRT) [36]. Geomechanical and geophysical analysis were also carried out in correspondence with the coastal granite rock mass underlying the wreck in order to assess its general stability [37]. In particular, from 25 January to 1 March 2012, an innovative experimental IRT monitoring campaign was carried out to assess the thermal behavior of the shipwreck and the surrounding sea stretch in order to locate possible thermal anomalies connected to deformations or oil spills. The salvage operations during their entire 30-month duration were a success, because the personnel involved in the rescue could rely on a solid warning in case of possible sliding of the wreck, and few pollutions were produced, even during the defueling. Furthermore, the analysis of the surface temperature variations of the deck contributed to the understanding of the vessel deformation trend. The aim of this paper is to present the lesson learned during the IRT monitoring in this complex emergency management, in order to provide useful outcomes regarding the contribution of thermal sensors analysis in shipwreck monitoring, and in the broader perspective of improving a still not well-developed scientific literature in the field of marine environmental disaster response.

## 2. Materials and Methods

InfraRed Thermography (IRT) is a versatile and low-cost, non-destructive diagnostic technique, accomplished with calibrated infrared thermal cameras capable of measuring with high spatial and temporal resolution the surface temperature pattern of the monitored scenarios [38].

The product of an IRT survey is a digital image acquired by the camera array detector (called “thermogram” or “thermographic image”), which, following the correction of the sensitive parameters, is converted by the camera's built-in processor into a surface temperature map [39]. The presence of any inhomogeneity within the surveyed material (e.g., an oil coating) highly modifies the material thermal parameters (density, specific heat, and thermal conductivity), reducing the heat transfer and adding its signal to that given by the structure [40]; therefore, the inhomogeneity is displayed in the analyzed surface temperature map as a thermal anomaly (an irregular thermal pattern with respect to the

surrounding areas) [41]. Modern high-resolution thermal cameras used both in terrestrial- (hand-held and tripod-mounted) or airborne-based modes, thanks to their portability and easy data collection/processing, represent powerful and cost-effective tools for thermal surveying and monitoring [42]. During the last decades, thanks to the technological development of portable high-resolution and cost-effective devices, IRT has been widely used in the field of civil engineering, cultural heritage, volcanic monitoring, environmental applications, and engineering geology [41–51].

#### *The Costa Concordia Shipwreck IRT Monitoring*

The IRT monitoring of the shipwreck was performed in tripod-mounted mode using a FLIR system SC620 thermal camera with a focal plane array (FPA) microbolometer sensor [52] (Figure 2; Table 1). A built-in 3.2 Mpixel digital camera allowed for the comparison between the thermograms and the corresponding optical images, in order to improve the interpretation of the thermal data.

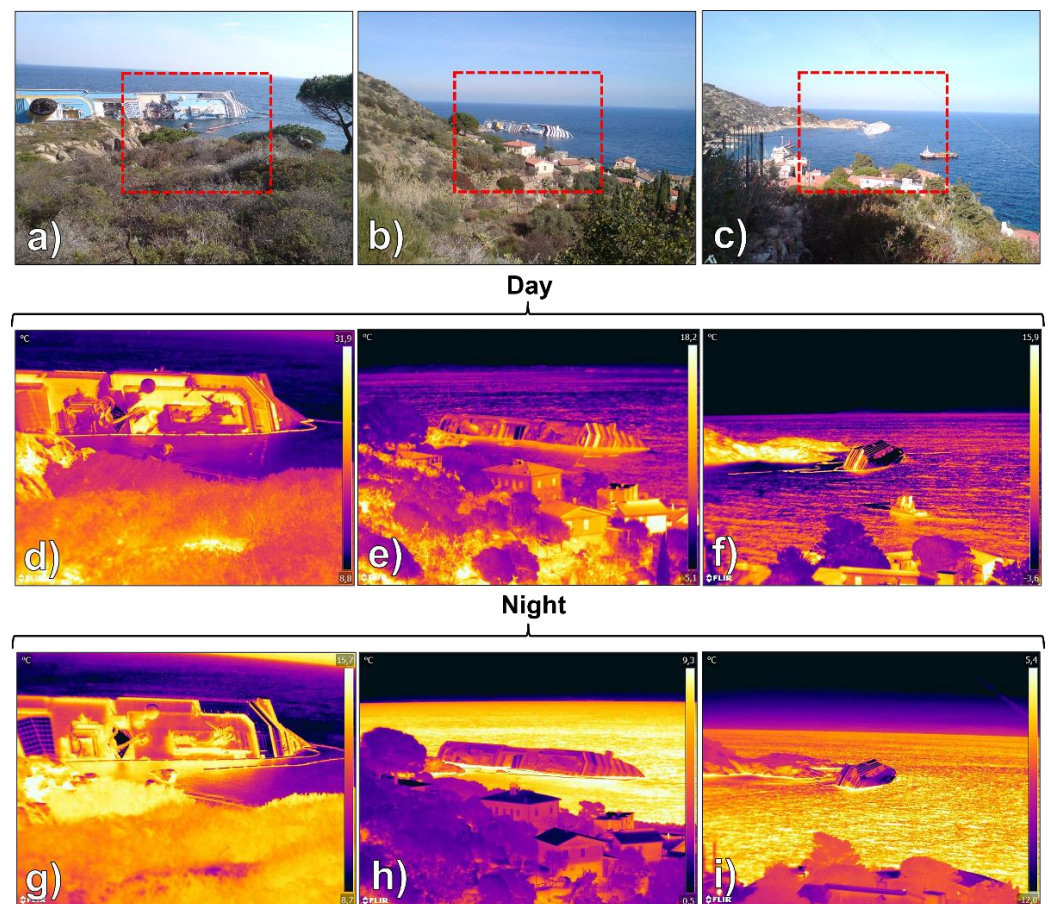


**Figure 2.** View of the Costa Concordia wreck from the acquiring points, showing the IR field of view (red dashed squares): (a) P1; (b) P2; (c) P3; examples of IRT thermograms during daytime from P1 (d), P2 (e); P3 (f), and during nighttime from P1 (g); P2 (h); P3 (i) (colorbar “iron”).

**Table 1.** Technical features of the adopted thermal camera and IRT survey parameters.

Spectral Range ( $\mu\text{m}$ )	Thermal Sensitivity (mK)	Sensor Spatial Resolution (mrad)	IR Resolution (pix)	Field of View ( $^{\circ}$ )	Sensor-Target Distance (m)	Image Resolution (m)
7.5–13	40	0.65	640 $\times$ 480	24 $\times$ 18	250 (P1); 700 (P2); 800 (P3)	1.6 (P1); 4.55 (P2); 5.20 (P3)

Data correction, thermal focusing, histogram equalization, and mosaicking were performed by means of FLIR Tools + software [53]. Through the thermographic survey, it was possible to measure the thermal radiation emitted by the ship and record the presence of any thermal anomalies in correspondence with the wreck and in the adjacent sea stretch. Initially, two acquisitions were made daily from three different acquisition points (P1–3 in Figure 1a), leading to an image resolution ranging from 1.6 m (P1) to 5.2 m (P3) (Table 1). Depending on their acquiring location, each thermogram was calibrated using the distance values and air temperature-humidity acquired through a pocket thermohygrometer, and a standard emissivity value of 0.95 (due to the complex multi-material scenario, as recommended by FLIR systems). In order to picture the daily temperature variations, two acquisitions were carried out around 12:00 and 00:00. Furthermore, from P1 (acquisition distance of approximately 250 from the shipwreck at a height of 26 m a.s.l.), between 5 to 29 February 2012, a short-term monitoring was also carried out by acquiring a thermogram every two hours approximately during daylight (Figure 2c). The aim was to analyze the surface temperature variations of the Costa Concordia deck, with the aim of assessing the possible effect of thermal dilatation on the vessel deformations (Figure 2d). The average temperatures variations in six distinct areas of the deck were calculated by means of a semi-automated processing procedure in a GIS environment [54]. The thermograms were converted to raster format, co-registered, and analyzed using the ArcGIS “zonal statistics tool”. Furthermore, in September 2013 and July 2014, during the parbuckling and hull removal operations (Figure 1e,f), an IR video sequence were also acquired, carried out from a fixed installation in P1 (Figure 2a,b) (Figure 2). By using FLIR ResearchIR software [55], single frames were then extracted and analyzed. The acquisition points P2 and P3 (distance of approximately 700 and 800 m from the shipwreck, and a height of 97 and 40 m a.s.l., respectively) were chosen to monitor the sea stretch surrounding the wreck for the detection of possible oil spills (Figure 2e).

### 3. Results

The bridge deck temperature measurements acquired in P1 are shown in Figure 3, together with the six control areas on the ship deck (Areas 1–6 in Figure 3a), their average temperature evolution (Figure 3b), and the air temperature recorded by the Giglio Porto air thermometric station (Figure 3c) [56]. The monitoring highlighted daily surface temperature peaks between 2 and 4 p.m. (values ranging approximately from 24.7 to 44.2 °C, in correspondence with Area 2), while the lowest values were recorded in correspondence with Area 4 (from 8.7 to −4.4 °C). Both areas are located on the left deck side; this difference is likely related to the different materials involved. The surface temperature differences plot shows also a higher thermal inertia for Area 2 and 6 (this latter is in the same material with respect to A3, but on the deck’s right sector, right above the sea water; Figure 3c). The high temperature range measured in all the control areas (Figure 3a,b) is much higher than the air temperature (Figure 3e); this result is due to the solar radiation of the extensive metal surface of the ship; the high specific heat of aluminum, widely used in the construction deck of the vessel, enhanced the storage of energy radiated by the sun and, thus, reached higher temperatures than air. This may have implied millimetric deformations of the shipwreck due to the linear thermal dilatation of the aluminum (Figure 3d).

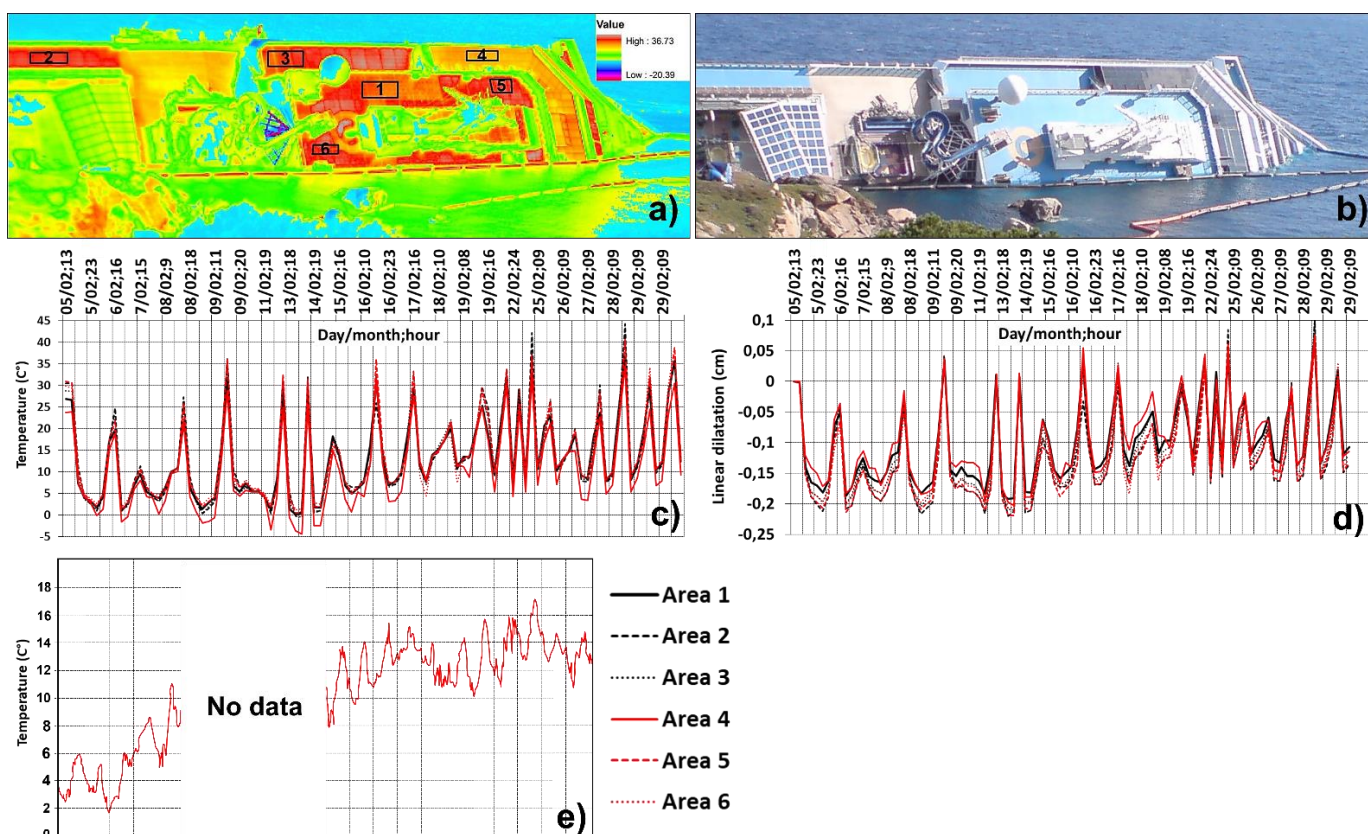


**Figure 3.** The IRT short-term monitoring campaign from P1: thermographic  $\Delta T$  Image of the deck sector with the control areas (1–6) created in ArcMap (a); corresponding optical image (see the collapsed glass panels of the deck) (b); average surface temperature variations in correspondence of the control areas (c); linear thermal dilatation in the control sectors (d); air temperature data of the marine weather station of Giglio Porto between 5 and 26 February 2012 (e). Time scale of panel (e) is the same with respect to subfigures (c,d).

This trend was confirmed by the correlation between the long-term RTS deformation measurements and the air temperature [33,36]. The IRT data collected from P2, and especially from P3, allowed detecting on 3 February 2012 around 00:40 and 12:00, as well as on 4 February 2012 at 00:00, cold thermal anomalies in the stretch of sea between the Costa Concordia shipwreck and Giglio harbor (2–3 °C lower than the surrounding sea water) (Figure 4). Already on 5 February 2012, the spill had ceased. On 1 February 2012, the anti-pollution floating booms surrounding the wreck during the defueling operation had been temporarily cut by the collapse of the deck's glass panels, allowing for oily substances to drift towards the island's harbor, as also confirmed by visual inspections (see Figure 3b). Yet, since there had been no hydrocarbon nor engine oil spills during the defueling operation, considering the extent of the oil slicks (around 30 m in maximum width for around 600 m in maximum length), and since its source point was the vessel's stern, where the kitchens of the restaurant rooms were located, this slick was interpreted as the leak of alimentary oily substances from the vessel's kitchens. Single thermograms, extracted and analyzed from the IR sequence recorded during the parbuckling operations on the night of 3 September 2012, showed that following the very first stages of the wreck righting, thermal anomalies in correspondence with jets of pressurized fluids were coming from the stern-side and the bow-side of the chimney (Figure 5). These fluids show temperatures between 22.1 °C (Figure 5a) and 19.9 °C (Figure 5b), suggesting that these could be interpreted as sea water jets developed in the peculiar fluid circulation within the wrecked vessel.

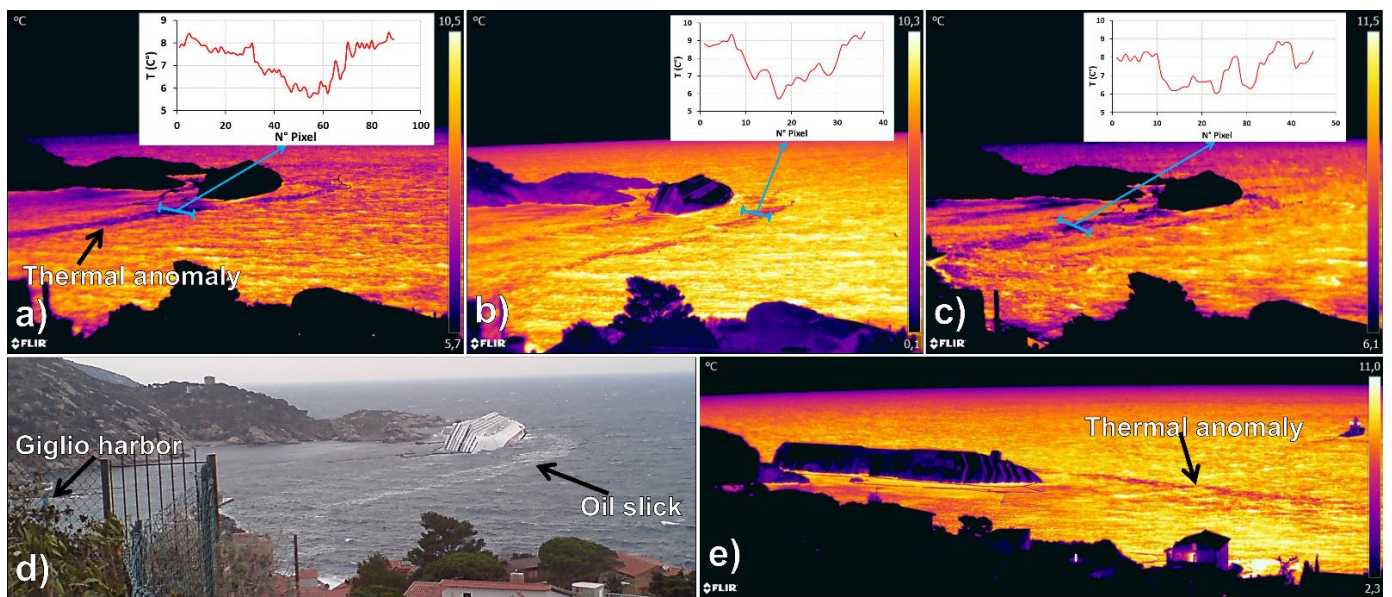


**Figure 4.** IRT applied for oil slick detection during the defueling operations (colorbar “iron”). Thermograms acquired from P3 on 3 February 2012 at 00:40 (a) and 12:30 (b); thermogram acquired from P3 on 4 February 2012 at 00:00 (c); correspondent optical image of b (d); mosaicked thermogram acquired from P2 on 3 February 2012 at 00:40 (e).

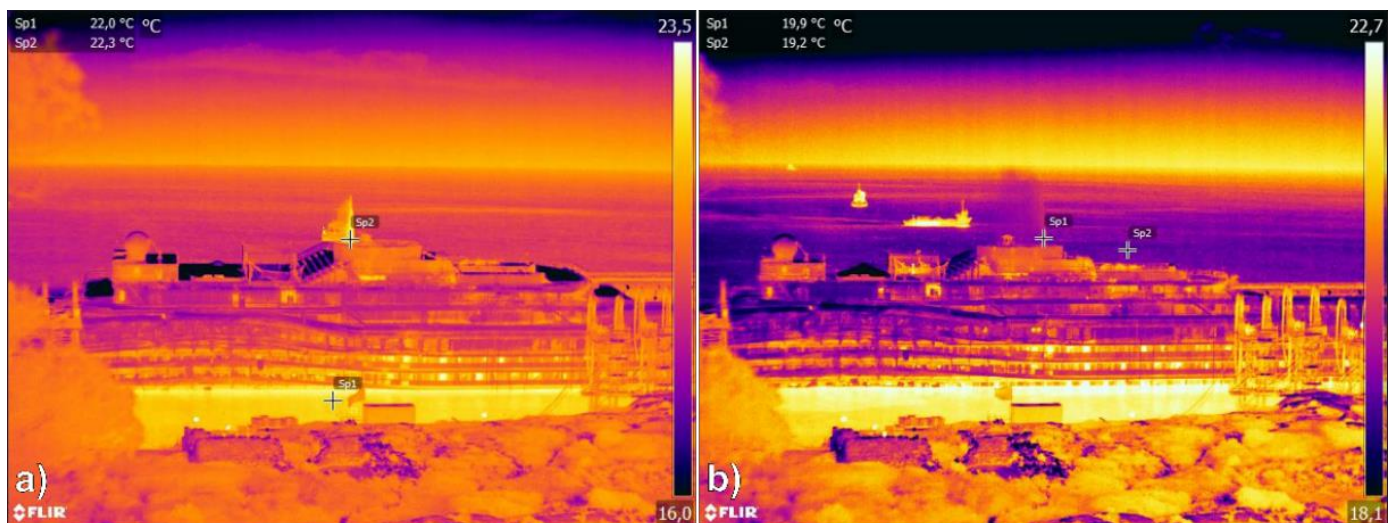


**Figure 5.** Thermograms selected from the IR video sequence acquired during the parbuckling (colorbar “iron”). Thermogram acquired at 02:42 on 17 September 2013 (a); thermogram acquired the same day at 04:12 (b) (Sp1–2 represent the spot measurements of single pixels).

In fact, sea water temperature in the warm sea stretch between the wreck and the coastline shows temperatures around 22 °C (the same of the first jet), whereas the slightly colder stretch facing the sea reaches around 19 °C (the same as the second jet) (Figure 5b).

This is probably due to the gradual temperature equilibrium reached between the first and second jet (which occurred with a time interval of around one hour and a half), following the new infilling of sea water in the sunken vessel during the initial phases of the righting. During the hull removal operations in the sea area between the coastline and the ship, no significant thermal anomalies possibly connected to oil spills were detected, as shown by the recorded IR video sequence acquired on 14 July 2014 (see Supplementary materials).

#### 4. Discussion

The Costa Concordia shipwreck salvage operations and its monitoring system represent an extraordinary effort in maritime history, considering the tonnage (114,137 gross registered tonnage) and the size of the ship (290 m in length, 70 in height, and 35 in width height). At the time of the wreckage, 2400 tons of fuel oil were stored inside the tanks, as were several other different pollutants potentially dangerous for the marine environment (e.g., engine oil, alimentary oil, and soap) [5]. For the authorities involved in the emergency management, this was the most alarming threat, together with the possible sliding of the wrecked ship from Punta Gabbianara and subsequent sinking in the deeper seabed, keeping in mind the concern for the security of the operators involved in the rescue and the body recovery. To the complexity of the scenario, it has to be added that several explosive charges were used to penetrate the deformed corridors and rooms of the vessel, which could lead to the potential instability of the wreck. The use of optical satellite remote sensing for oil spills is improving, although its success is generally limited to identifying features at sites where known oil spills have occurred, and it can be profitably used as a base to add other sensors' information (oil shows no spectral characteristics in the visible region) [5]. SAR surely offers the only potential for large area searches and adverse weather remote sensing [57]. Nevertheless, SAR is often costly, its efficiency connected to the revisit time of the satellite, and it is prone to many interferences (false targets can be as high as 95%) [4,5]. In recent years, these limitations can be in part hampered using ESA's Sentinel data, although these are provided only for the European area. Laser fluor sensor is probably the most effective sensor for positively discriminating oil on most backgrounds that include water, soil, ice, and snow; nevertheless, it needs an airborne platform and may be costly [58]. Although there are not still many examples in the literature, IRT from terrestrial and UAV platforms seems to be an ideal tool to detect environmental contamination since, e.g., in oil films on water, it can reduce its surface temperature, therefore representing a thermal anomaly [59]. Furthermore, regarding the monitoring of the hull's thermally induced deformations, the use of wireless sensor networks (WSN) could also have promising results, as shown in several successful applications in the field of disaster risk management [60–62]. In this work, the applicability and potential of IRT as a novel operational tool in a multiparametric and multiplatform shipwreck monitoring system was tested. The results show that although its applications in the field of maritime disaster management are still experimental, IRT can be profitably used in different emergency phases to monitor the vessel thermally induced deformation and small oil spills in the sea stretches surrounding the wreck. In particular, regarding the outcomes of the Costa Concordia monitoring [36], during the first defueling and caretaking phases (up to 1 September 2012), the recorded surface temperature was correlated to the periodic daily thermal dilatations (Figure 3). Temperature did not seem to directly influence the deformations related to accelerations, which in turn were related to tidal, wind, and storm wave effects [36]. IRT showed its potential in detecting between 3 and 4 February 2012 a thermal anomaly of 2 °C with respect to the surrounding sea stretch that was confirmed to be an oil spill coming from the vessel's stern, drifting towards the island harbor (Figure 4). Therefore, a prompt warning was sent to the authorities and personnel involved in the emergency management. During the experimental monitoring, IRT has proven to be a versatile tool, not only for its night vision (e.g., during the parbuckling phase), but also for the capability of the thermal camera to work in a rapid installation-acquisition approach from different points of view and acquiring modes (e.g., from single thermograms to IR video sequences, as in both the parbuckling and hull removal phase) (Figure 5 and Supplementary materials). P1 was the only feasible location for close-range monitoring from a fixed point (the thermal camera was in fact installed together with other instruments of the integrated monitoring system in a cabin-hut with electric power supply) (Figures 1 and 2a,b,e,h). P3 instead granted a favorable commanding view, being on the hilltop just south of Giglio Porto village, overlooking the sea stretch between the wreck and the island harbor (Figures 1 and 2d,g,i).

In this framework the Giglio island's geomorphological setting (relatively steep hilly coastline) granted favorable monitoring point of views with respect to lower flat coastlines. IRT also showed its versatility by detecting after rainfall events cold thermal anomalies connected to seepage along key rock mass discontinuities (granite exfoliation slope-dipping joints) (Figure 6). This represents valuable information, since seepage is an important factor in reducing the wall strength of discontinuities [63], and the most important potential instability phenomena detected in the area by means of rock mass kinematic analysis [51] were plane failures along exfoliation joints, but also because it represents an input for the modelling of the rock mass stability activities [37].

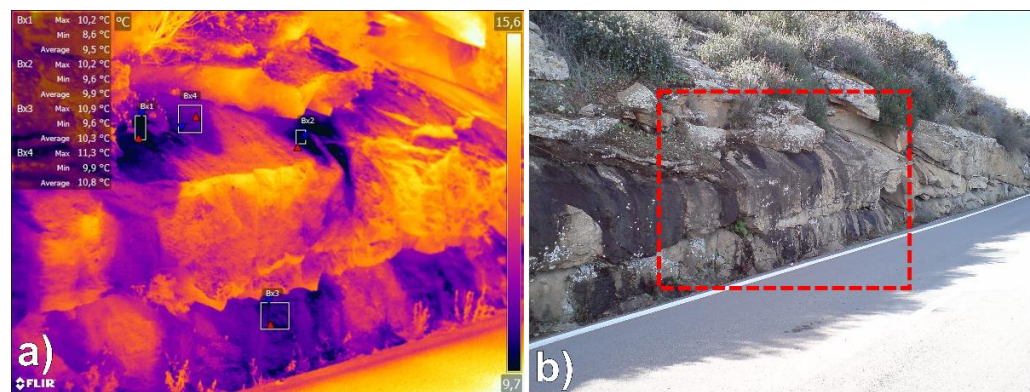


**Figure 6.** Rock mass IRT survey (colorbar “iron”). Cold thermal anomalies in correspondence of granite exfoliation joints (a); correspondent visible image (b) (red dashed square highlight the camera field of view).

Furthermore, the possibility to use box plots (Bx1–4 in Figure 6a) for areal surface temperature measurements shows how IRT can not only detect seepage-affected areas (Bx1 and 2), but also potentially discriminate on the discontinuity of the dampness rating and the evidence of water flow, based on the surface temperature (e.g., Bx3–4 in Figure 6a) [50,51]. The timing and the number of daily acquisitions was restricted by the operative and logistic limitations: only a single thermal camera was available, and the dedicated personnel was compelled to assemble daily all the integrated monitoring system data to produce bulletins for the National Civil Protection Department. Furthermore, 24 h IR sequences from fixed installations would have produced a huge amount of data (one minute of IR-video with 60 frames per second is about 1.8 Gigabyte), creating serious data management problems. IRT alone is insufficient for an effective shipwreck monitoring, since it can only detect surface temperature changes; nevertheless, this work showed how this kind of information can be profitably used in integration with other techniques devoted to monitoring the deformations (e.g., RTS and SAR).

## 5. Conclusions

In conclusion, this work represents an important novel experimental application of IRT in maritime disaster management. Between 3–4 February, IRT successfully detected on oil spill drifting from the stern of the wreck towards the island harbor. Close-range IRT monitoring revealed the wreck thermal dilatation, providing interesting insights for the interpretation of the monitored deformation data. This work shows that IRT can be profitably used in maritime salvage as an ancillary low-cost technique, which can be used operatively in an integrated multiplatform and multi-sensor shipwreck monitoring system with other ground-based remote sensing techniques, such as optical imagery, lidar, and spaceborne and ground-based SAR. Nevertheless, in order to obtain an accurate interpretation of the results, a skilled operator is highly recommended. Future developments in maritime disaster response should include the application of IRT from unmanned UAV platforms

and from fixed thermal camera installations for gathering continuous, high-resolution, real-time data.

**Supplementary Materials:** The following supporting information can be downloaded at: <https://www.mdpi.com/article/10.3390/rs15051347/s1>, two IR video sequences acquired on 14 July 2014, during the hull removal operations. IR Video S1: 2014-07-14T113854906; IR Video S2: 2014-07-14T150751558.

**Author Contributions:** W.F. conceived the structure, elaborated the thermal data, wrote the paper, and designed the figures. G.R., L.T. and A.R. conceived the short-term thermal monitoring from P1 position and set the procedure for the data semi-automatic analysis. F.M. and L.L. acquired the IR video sequence during the parbuckling and hull removal operations, respectively. R.F. and N.C. coordinated the research. All authors have read and agreed to the published version of the manuscript.

**Funding:** This research was carried out in the framework of the agreement with the Department of Earth Sciences of the University of Florence (Italy) “Monitoring of the Costa Concordia (Giglio Island)” on behalf of the Commissioner delegate of the Presidency of the Council of Ministers ex OPCM 3998/2012, funded by the Italian Civil Protection Department.

**Data Availability Statement:** Not applicable.

**Acknowledgments:** The authors would like to thank the Italian Civil Protection Department and all the current and former colleagues from the Department of Earth Sciences of the University of Florence (Italy) who were involved in the Costa Concordia shipwreck monitoring (in alphabetical order): Federica Bardi, Alessandro Battistini, Silvia Bianchini, Andrea Ciampalini, Federico Di Traglia, Giulia Dotta, Federica Ferrigno, Francesco Fidolini, Sara Frangioni, Francesca Garfagnoli, Emanuele Intrieri, Daniela Lagomarsino, Alessia Lotti, Stefano Morelli, Massimiliano Nocentini, Teresa Nolesini, Veronica Pazzi, Federico Raspini, Samuele Segoni, Carlo Tacconi Stefanelli and Deodato Tapete.

**Conflicts of Interest:** The authors declare no conflict of interest.

## References

1. Ivanov, A.Y. The oil spill from a shipwreck in Kerch Strait: Radar monitoring and numerical modelling. *Int. J. Remote Sens.* **2010**, *31*, 4853–4868. [[CrossRef](#)]
2. Pisano, A.; Bignami, F.; Santoleri, R. Oil spill detection in glint-contaminated near-infrared MODIS imagery. *Remote Sens.* **2015**, *7*, 1112–1134. [[CrossRef](#)]
3. Chen, X.; Liu, S.; Liu, R.W.; Wu, H.; Han, B.; Zhao, J. Quantifying Arctic oil spilling event risk by integrating an analytic network process and a fuzzy comprehensive evaluation model. *Ocean Coast. Manag.* **2022**, *228*, 106326. [[CrossRef](#)]
4. Lodge, A.E. *The Remote Sensing of Oil Slicks*; John Wiley & Son: Chichester, UK, 1989; p. 147. ISBN -0471920436.
5. Ciampalini, A.; Raspini, F.; Bianchini, S.; Tarchi, D.; Vespe, M.; Moretti, S.; Casagli, N. The Costa Concordia last cruise: The first application of high frequency monitoring based on COSMO-SkyMed constellation for wreck removal. *ISPRS J. Photogramm. Remote Sens.* **2016**, *112*, 37–49. [[CrossRef](#)]
6. Fingas, M.; Brown, C. Review of oil spill remote sensing. *Mar. Pollut. Bull.* **2014**, *83*, 9–23. [[CrossRef](#)] [[PubMed](#)]
7. Martinez, A.; Moreno, V. An oil spill monitoring system based on SAR images. *Spill Sci. Technol. Bull.* **1996**, *3*, 65–71. [[CrossRef](#)]
8. Montero, P.; Blanco, J.; Cabanas, J.M.; Maneiro, J.; Pazos, Y.; Moróño, A.; Montero, P.; Balseiro, C.F.; Carracedo, P.; Gomez, B.; et al. Oil spill monitoring and forecasting on the Prestige-Nassau accident. In *Arctic and Marine Oilspill Program Technical Seminar*; Environment Canada: Toronto, ON, Canada, 2003; Volume 2, pp. 1013–1030.
9. Brekke, C.; Solberg, A.H. Oil spill detection by satellite remote sensing. *Remote Sens. Environ.* **2005**, *95*, 1–13. [[CrossRef](#)]
10. Zhang, Y.; Lin, H.; Liu, Q.; Hu, J.; Li, X.; Yeung, K. Oil-spill monitoring in the coastal waters of Hong Kong and vicinity. *Mar. Geod.* **2012**, *35*, 93–106. [[CrossRef](#)]
11. Rogne, T.; MacDonald, I.; Smith, A.; Kennicutt, M.C.; Giammona, C.S. Multispectral remote sensing and truth data from the Tenyo Maru oil spill. *Photogramm. Eng. Remote Sens.* **1993**, *59*, 3.
12. Grimaldi, C.S.L.; Casciello, D.; Coviello, I.; Lacava, T.; Pergola, N.; Tramutoli, V. An improved RST approach for timely alert and Near Real Time monitoring of oil spill disasters by using AVHRR data. *Nat. Hazards Earth Syst. Sci.* **2011**, *11*, 1281. [[CrossRef](#)]
13. Maianti, P.; Rusmini, M.; Tortini, R.; Dalla Via, G.; Frassy, F.; Marchesi, A.; Rota Nodari, F.; Gianinetto, M. Monitoring large oil slick dynamics with moderate resolution multispectral satellite data. *Nat. Hazards* **2014**, *73*, 473–492. [[CrossRef](#)]
14. Balogun, A.L.; Yekeen, S.T.; Pradhan, B.; Althuwaynee, O.F. Spatio-Temporal Analysis of Oil Spill Impact and Recovery Pattern of Coastal Vegetation and Wetland Using Multispectral Satellite Landsat 8-OLI Imagery and Machine Learning Models. *Remote Sens.* **2020**, *12*, 1225. [[CrossRef](#)]
15. Li, Y.; Liu, Y.; Ma, L.; Li, X. Oil Spill Monitoring Using MODIS Data. In *Second International Conference on Space Information Technology*; International Society for Optics and Photonics: Bellingham, WA, USA, 2007; Volume 6795, p. 67955G.

16. Casciello, D.; Lacava, T.; Pergola, N.; Tramutoli, V. Robust Satellite Techniques for oil spill detection and monitoring using AVHRR thermal infrared bands. *Int. J. Remote Sens.* **2011**, *32*, 4107–4129. [[CrossRef](#)]
17. Xing, Q.; Li, L.; Lou, M.; Bing, L.; Zhao, R.; Li, Z. Observation of oil spills through landsat thermal infrared imagery: A case of deepwater horizon. *Aquat. Procedia* **2015**, *3*, 151–156. [[CrossRef](#)]
18. Allik, T.H.; Dixon, R.E.; Walters, M. Remote measurement of thick oil spill depth using thermal imagery. In Ocean Sensing and Monitoring X. *Int. Soc. Opt. Photonics* **2018**, *10631*, 106310F.
19. Fingas, M.F.; Brown, C.E. *Oil Spill Remote Sensors: Review, Trends and New Developments*; (No. CONF-970319-); The Environmental Research Institute of Michigan (ERIM): Ann Arbor, MI, USA, 1997.
20. Lehr, W.J.; Simecek-Beatty, D. The relation of Langmuir circulation processes to the standard oil spill spreading, dispersion, and transport algorithms. *Spill Sci. Technol. Bull.* **2000**, *6*, 247–253. [[CrossRef](#)]
21. Palmer, D.; Borstad, G.A.; Boxall, S.R.; House, R.; Quay, E. Airborne multispectral remote sensing of the January 1993 Shetlands oil spill. In Proceedings of the Second Thematic Conference on Remote Sensing for Marine and Coastal Environments: Needs, Solutions and Applications, New Orleans, LA, USA, 31 January–2 February 1994; pp. 546–558.
22. Shen, S.S.; Lewis, P.E. Deepwater Horizon oil spill monitoring using airborne multispectral infrared imagery. In Proceedings of the Algorithms and Technologies for Multispectral, Hyperspectral, and Ultraspectral Imagery XVII, Orlando, FL, USA, 25–28 April 2011; Volume 8048, p. 80480H.
23. Grierson, I.T. Use of airborne thermal imagery to detect and monitor inshore oil spill residues during darkness hours. *Environ. Manag.* **1998**, *6*, 905–912. [[CrossRef](#)]
24. Jha, M.N.; Levy, J.; Gao, Y. Advances in remote sensing for oil spill disaster management: State-of-the-art sensors technology for oil spill surveillance. *Sensors* **2008**, *8*, 236–255. [[CrossRef](#)]
25. De Kerf, T.; Gladines, J.; Sels, S.; Vanlanduit, S. Oil spill detection using machine learning and infrared images. *Remote Sens.* **2020**, *12*, 4090. [[CrossRef](#)]
26. Goodman, R. Overview and future trends in oil spill remote sensing. *Spill Sci. Technol. Bull.* **1994**, *1*, 11–21. [[CrossRef](#)]
27. Robbe, N.; Hengstermann, T. Remote sensing of marine oil spills from airborne platforms using multi-sensor systems. *Water Pollut. VIII Model. Monit. Manag.* **2006**, *1*, 347–355.
28. Al-Ruzouq, R.; Gibril, M.B.A.; Shanableh, A.; Kais, A.; Hamed, O.; Al-Mansoori, S.; Khalil, M.A. Sensors, features, and machine learning for oil spill detection and monitoring: A review. *Remote Sens.* **2020**, *12*, 3338. [[CrossRef](#)]
29. Leifer, I.; Lehr, W.J.; Simecek-Beatty, D.; Bradley, E.; Clark, R.; Dennison, P.; Hu, Y.; Matheson, S.; Jones, C.E.; Holt, B.; et al. State of the art satellite and airborne marine oil spill remote sensing: Application to the BP Deepwater Horizon oil spill. *Remote Sens. Environ.* **2012**, *124*, 185–209. [[CrossRef](#)]
30. Zhao, J.; Temimi, M.; Ghedira, H.; Hu, C. Exploring the potential of optical remote sensing for oil spill detection in shallow coastal waters—a case study in the Arabian Gulf. *Opt. Express* **2014**, *22*, 13755–13772. [[CrossRef](#)] [[PubMed](#)]
31. Schröder-Hinrichs, J.U.; Hollnagel, E.; Baldauf, M. From Titanic to Costa Concordia—A century of lessons not learned. *WMU J. Marit. Aff.* **2012**, *11*, 151–167. [[CrossRef](#)]
32. Fiaschi, A.; Matassoni, L.; Lotti, A.; Saccorotti, G. Micro-seismic monitoring after the shipwreck of the Costa Concordia at Giglio Island (Italy). *Acta Geophys.* **2017**, *65*, 1019–1027. [[CrossRef](#)]
33. Manconi, A.; Allasia, P.; Giordan, D.; Baldo, M.; Lollino, G. Monitoring the Stability of Infrastructures in An Emergency Scenario: The “Costa Concordia” Vessel Wreck. In *Global View of Engineering Geology and the Environment*; Taylor & Francis Group: London, UK, 2013.
34. Raspini, F.; Moretti, S.; Fumagalli, A.; Rucci, A.; Novali, F.; Ferretti, A.; Claudio Prati, C.; Casagli, N. The COSMO-SkyMed constellation monitors the Costa Concordia wreck. *Remote Sens.* **2014**, *6*, 3988–4002. [[CrossRef](#)]
35. Broussolle, J.; Kyovtorov, V.; Basso, M.; Castiglione, G.F.D.S.E.; Morgado, J.F.; Giuliani, R.; Olivero, F.; Sammartino, P.F.; Tarchi, D. MELISSA, a new class of ground based InSAR system. An example of application in support to the Costa Concordia emergency. *ISPRS J. Photogramm. Remote Sens.* **2014**, *91*, 50–58. [[CrossRef](#)]
36. Casagli, N.; Moretti, S.; Gabbani, G.; Catani, F.; Fanti, R.; Agostini, A.; Bardi, F.; Battistini, A.; Bianchini, S.; Ciampalini, A.; et al. *Monitoraggio Della Costa Concordia (Isola Del Giglio)—Rapporto Finale. Presidenza Del Consiglio Dei Ministri—Dipartimento Della Protezione Civile*; Internal Report; Earth Science Department, University of Florence: Florence, Italy, 2014. (In Italian)
37. Dotta, G.; Gigli, G.; Ferrigno, F.; Gabbani, G.; Nocentini, M.; Lombardi, L.; Agostini, A.; Nolesini, T.; Casagli, N. Geomechanical characterization and stability analysis of the bedrock underlying the Costa Concordia cruise ship. *Rock Mech. Rock Eng.* **2017**, *50*, 2397–2412. [[CrossRef](#)]
38. Maldague, X. *Theory and Practice of Infrared Technology for Non-Destructive Testing*; John-Wiley & Sons: Hoboken, NJ, USA, 2001; 684p.
39. Spampinato, L.; Calvari, S.; Oppenheimer, C.; Boschi, E. Volcano surveillance using infrared cameras. *Earth-Sci. Rev.* **2011**, *106*, 63–91. [[CrossRef](#)]
40. Ludwig, N.; Redaelli, V.; Rosina, E.; Augelli, F. Moisture detection in wood and plaster by IR thermography. *Infrared Phys. Technol.* **2004**, *46*, 161–166. [[CrossRef](#)]
41. Teza, G.; Marcato, G.; Castelli, E.; Galgaro, A. IRTROCK: A MATLAB toolbox for contactless recognition of surface and shallow weakness of a rock cliff by infrared thermography. *Comput. Geosci.* **2012**, *45*, 109–118. [[CrossRef](#)]

42. Frodella, W.; Gigli, G.; Morelli, S.; Lombardi, L.; Casagli, N. Landslide mapping and characterization through infrared thermography (IRT): Suggestions for a methodological approach from some case studies. *Remote Sens.* **2017**, *9*, 1281. [CrossRef]
43. Wu, J.H.; Lin, H.M.; Lee, D.H.; Fang, S.C. Integrity assessment of rock mass behind the shotcreted slope using thermography. *Eng. Geol.* **2005**, *80*, 164–173.
44. Hardgrove, C.; Moersch, J.; Whisner, S. Thermal imaging of sedimentary features on alluvial fans. *Planet. Space Sci.* **2010**, *58*, 482–508. [CrossRef]
45. Frodella, W.; Morelli, S.; Fidolini, F.; Pazzi, V.; Fanti, R. Geomorphology of the Rotolon landslide (Veneto region, Italy). *J. Maps* **2014**, *10*, 394–401. [CrossRef]
46. Pappalardo, G.; Mineo, S.; Zampelli, S.P.; Cubito, A.; Calcaterra, D. InfraRed Thermography proposed for the estimation of the Cooling Rate Index in the remote survey of rock masses. *Int. J. Rock Mech. Min. Sci.* **2016**, *83*, 182–196. [CrossRef]
47. Di Traglia, F.; Nolesini, T.; Solari, L.; Ciampalini, A.; Frodella, W.; Steri, D.; Allotta, B.; Rindi, A.; Marini, L.; Monni, N.; et al. Lava delta deformation as a proxy for submarine slope instability. *Earth Planet. Sci. Lett.* **2018**, *488*, 46–58. [CrossRef]
48. Guerin, A.; Jaboyedoff, M.; Collins, B.D.; Derron, M.H.; Stock, G.M.; Matasci, B.; Boesiger, M.; Lefevvre, C.; Podladchikov, Y.Y. Detection of rock bridges by infrared thermal imaging and modeling. *Sci. Rep.* **2019**, *9*, 1–19. [CrossRef]
49. Frodella, W.; Elashvili, M.; Spizzichino, D.; Gigli, G.; Adikashvili, L.; Vacheishvili, N.; Kirkitadze, G.; Nadaraia, A.; Margottini, C.; Casagli, N. Combining InfraRed Thermography and UAV Digital Photogrammetry for the Protection and Conservation of Rupestrian Cultural Heritage Sites in Georgia: A Methodological Application. *Remote Sens.* **2020**, *12*, 892. [CrossRef]
50. Frodella, W.; Lazzeri, G.; Moretti, S.; Keizer, J.; Verheijen, F.G. Applying Infrared Thermography to Soil Surface Temperature Monitoring: Case Study of a High-Resolution 48 h Survey in a Vineyard (Anadia, Portugal). *Sensors* **2020**, *20*, 2444. [CrossRef] [PubMed]
51. Frodella, W.; Elashvili, M.; Spizzichino, D.; Gigli, G.; Nadaraia, A.; Kirkitadze, G.; Adikashvili, L.; Margottini, C.; Antidze, N.; Casagli, N. Applying Close Range Non-Destructive Techniques for the Detection of Conservation Problems in Rock-Carved Cultural Heritage Sites. *Remote Sens.* **2021**, *13*, 1040. [CrossRef]
52. FLIR Systems Inc. FLIR ThermoCAM SC620 Technical Specifications. 2009. Available online: [www.flir.com/cs/emea/en/view/?id=41965](http://www.flir.com/cs/emea/en/view/?id=41965) (accessed on 22 December 2022).
53. FLIR Systems Inc. FLIR Tools + Datasheet. 2015. Available online: <https://www.infraredcamerawarehouse.com/content/FLIR%20Datasheets/FLIR%20ToolsPlus%20Datasheet.pdf> (accessed on 22 December 2022).
54. ESRI Inc. ArcMap 10.1 Datasheet. 2012. Available online: <https://www.esri.com/news/arcnews/spring12articles/introducing-arcgis-101.html> (accessed on 1 October 2019).
55. FLIR Systems Inc. ResearchIR 3.4. sp3. 2013. Available online: [http://support.flir.com/DsDownload/Assets/T198206\\_en\\_40.pdf](http://support.flir.com/DsDownload/Assets/T198206_en_40.pdf) (accessed on 1 June 2022).
56. Centro Funzionale Regione Toscana (CFR)—Termometria. Available online: <https://www.cfr.toscana.it/index.php?IDS=42&IDSS=278> (accessed on 1 December 2022).
57. Dassenakis, M.; Paraskevopoulou, V.; Cartalis, C.; Adaktilou, N.; Katsiabani, K. Remote sensing in coastal water monitoring: Applications in the eastern Mediterranean Sea (IUPAC Technical Report). *Pure Appl. Chem.* **2011**, *84*, 335–375. [CrossRef]
58. Tebeau, P.A.; Etkin, D.S.; French-McCay, D.P. *Cost-Benefit Analysis for Using Laser Fluorosensor for Detecting Heavy Oil*; Coast Guard Research and Development Center: Groton, CT, USA, 2006.
59. Lega, M.; Kosmatka, J.; Ferrara, C.; Russo, F.; Napoli, R.M.A.; Persechino, G. Using advanced aerial platforms and infrared thermography to track environmental contamination. *Environ. Forensics* **2012**, *13*, 332–338. [CrossRef]
60. Aziz, N.A.A.; Aziz, K.A. Managing disaster with wireless sensor networks. In Proceedings of the 13th International Conference on Advanced Communication Technology (ICACT2011), Gangwon-Do, Republic of Korea, 13–16 February 2011; pp. 202–207.
61. Erdelj, M.; Król, M.; Natalizio, E. Wireless sensor networks and multi-UAV systems for natural disaster management. *Comput. Netw.* **2017**, *124*, 72–86. [CrossRef]
62. Intriери, E.; Gigli, G.; Gracchi, T.; Nocentini, M.; Lombardi, L.; Mugnai, F.; Frodella, W.; Bertolini, G.; Carnevale, E.; Favalli, M.; et al. Application of an ultra-wide band sensor-free wireless network for ground monitoring. *Eng. Geol.* **2018**, *238*, 1–14. [CrossRef]
63. ISRM. Suggested methods for the quantitative description of discontinuities in rock masses. *Int. J. Rock Mech. Min. Sci. Geomech. Abstr.* **1978**, *15*, 319–368.

**Disclaimer/Publisher’s Note:** The statements, opinions and data contained in all publications are solely those of the individual author(s) and contributor(s) and not of MDPI and/or the editor(s). MDPI and/or the editor(s) disclaim responsibility for any injury to people or property resulting from any ideas, methods, instructions or products referred to in the content.